Homogenization of the Equations Governing the Flow Between a Slider and a Rough Spinning Disk

Industry Participants: F. Hendriks and K. Rubin (Hitachi)

University Contributors:

D. Cargill, J. Fehribach, T-S. Lin, C. Please, C. Raymond, D. Schwendeman, T. Skorczewski, B. Tilley, T. Witelski, J. Wróbel, J. Wang and S. Zhang

July 28, 2009

1 Introduction

The main challenge in the design of hard-disk drives is to increase the density of data storage. Traditional disk-drive designs involve a read/write head positioned on a slider bearing that flies over a smooth spinning magnetic disk. The demand for larger data storage has made it necessary to reduce the minimum gap height for various design features of the air-bearing surface to be in the range of tens of nanometers to just a few nanometers in present-day drives. A further reduction in the minimum gap height has become physically impractical so that in future designs other approaches may be used. One approach is to use "patterned" magnetic disks in which the disk is rough on the nanometer scale. A potential difficulty in the design process for such patterned disks is that the behavior of the flow in the gap may no longer be described with sufficient accuracy by the solution of the compressible Reynolds equation in lubrication theory. Since many flow solutions are needed in the inner loop of the design process, discarding the numerical solution of the Reynolds equation in favor of the numerical solution of the full Navier-Stokes equations implies a huge increase in computational cost. Thus, a significant problem of interest to Hitachi is whether modified versions of the Reynolds equation may be derived for patterned disks using some asymptotic homogenization approach, and whose solutions provide sufficient accuracy for the design process.

Figure 1 shows a schematic of a patterned disk. The slider bearing is located at the end of a suspension structure that acts in a manner of a tone-arm support to control the radial position of the slider as it flies over the spinning disk. The patterned disk has regions of concentric grooves and discrete islands, the former representative of Discrete Track Media (DTM) while the later representative of Bit Patterned Media (BPM). For purposes of mathematical analysis we consider the two cases separately, and view DTM as *longitudinal roughness* running in the direction of the relative motion between the slider bearing and the disk, whereas we view BPM as *transverse roughness* running perpendicular to the relative motion, i.e. "speed bumps." Since the length scale of the roughness is on the order of nanometers which is much smaller than the millimeter length scale of the slider bearing, a homogenization of the equations governing the flow is considered for both cases.

In order to carry out a mathematical analysis of both cases, we need to consider the various parameters

Param.	Value	Param.	Value
U	25 m/s	h_0	10 nm
L	1 mm	λ	50 nm
ρ_a	1 kg/m^3	P_a	100 kPa
μ	10^{-5} Pa s		

Table 1: Parameter values.

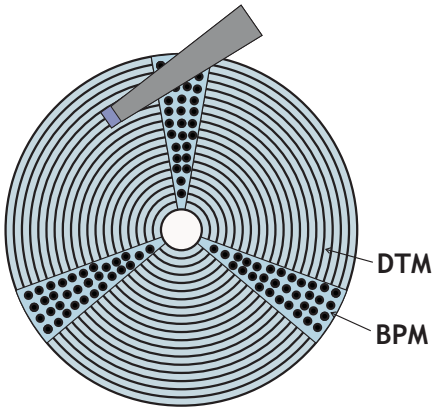

Figure 1: Schematic of a slider bearing (at the end of a tone-arm support) flying over a patterned disk. The patterned disk contains regions of concentric grooves (Discrete Track Media) and discrete islands (Bit Patterned Media).

of the problem. These parameters are collected in Table 1. Here U is a representative value for the speed of the slider relative to the disk, h_0 is the minimum gap height, L is the length scale for the slider, λ is a length scale for the roughness along the surface of the disk (see Figures 2 and 5), and ρ_a, P_a and μ are ambient values for the density, pressure and dynamic viscosity of the flow, respectively. From these, we can construct several relevant dimensionless parameters, namely,

$$\mathrm{Re}^* = \frac{\rho_a U L}{\mu}\left(\frac{h_0}{L}\right)^2 = 2.5\times 10^{-7}, \quad \Lambda = \frac{6\mu U L}{P_a h_0^2} = 1.5\times 10^{5}, \quad \delta = \frac{h_0}{L} = 10^{-5}, \quad \epsilon = \frac{\lambda}{L} = 5\times 10^{-5}$$

which are, respectively, the reduced Reynolds number, the bearing number, the ratio of the minimum gap height to the slider length, and the ratio of the length scale of the roughness to that of the slider. The reduced Reynolds number is very small and allows us to neglect the convective terms in the Navier-Stokes equations to a good approximation. A further reduction for large bearing number may also be considered, but this is not done in the analysis below (except for the brief discussion in Section 3.1). We do make use of that fact that both δ and ϵ are small.

In the homogenization analysis that follows, we employ standard references on perturbation methods, such as the books by Hinch [1] and Holmes [2], and refer to previous work on the analysis of slider bearings by Witelski [3]. In particular, numerical codes developed by Witelski are used to obtain direct simulations of the gap pressure under a slider, and then compare them with corresponding solutions determined by the homogenized equations obtained in Section 3 below. We also note that others have considered the behavior of surface roughness on slider bearings, see for example, Jai and Bou-Saïd [4] and Hayashi, Yoshida and Mitsuya [5].

The remaining sections of the report are organized as follows. In Section 2, we consider the case of longitudinal roughness, and in Section 3 we consider the case of transverse roughness. Conclusions of our work are discussed in Section 4.

2 Longitudinal Roughness

Consider the flow of an isothermal gas flowing under a slider bearing shown in Figure 2. The coordinate system (x, y, z) is chosen in a reference frame that is stationary with the slider, with x being the direction of the motion of the lower surface, y being the spanwise coordinate, and z being the vertical coordinate. (We assume that the location of the slider is far from the center of the disk so that curvature effects are negligible.) The lower surface, moving at a speed U, is given by $z = H_1(y)$. It varies in the spanwise direction, but is uniform in the flow direction. The slider bearing is defined on $0 \le x, y \le L$ and is described by the surface

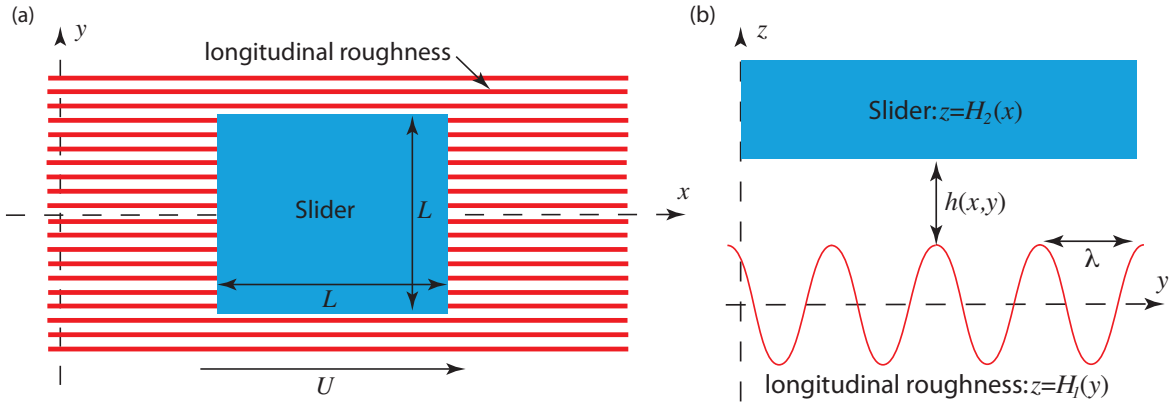

Figure 2: Flow geometry for the slider problem with longitudinal roughness: (a) top view of the slider with roughness underneath and (b) front view of the slider. The slider has length and width given by L and moves with speed U. The gap height is $h(x, y)$ and the period of the longitudinal roughness is λ.

$z = H_2(x)$. It varies in the flow direction, but is uniform in the spanwise direction. We are interested in describing the steady pressure field p and the gas fluid velocity $\vec{u}$ in the space between the slider and the lower surface. In the following subsection, we describe an asymptotic analysis of the problem. Sample calculations of the asymptotic equations are given in the subsection after that.

2.1 Asymptotic analysis

The flow in the gap is described by the steady compressible Navier-Stokes equations. The equations consist of mass conservation

$$\nabla \cdot [\rho \vec{u}] = 0 \,, \tag{1}$$

where ρ is the fluid density, and a momentum balance given by

$$\rho \vec{u} \cdot \nabla \vec{u} + \nabla p = \mu \left\{ \nabla^2 \vec{u} + \frac{1}{3} \nabla \left[\nabla \cdot \vec{u} \right] \right\} \,, \tag{2}$$

where μ is the dynamic viscosity of the air. Gravitational effects in the fluid are considered to be negligible and are not considered here. Finally, we need an equation of state relating the gas pressure to its density, and for simplicity we consider the ideal gas law

$$p = \rho R T \,, \tag{3}$$

where R is a gas constant and T is a constant temperature. The boundary conditions consist of no-slip boundary conditions along the solid surfaces

$$\begin{aligned} u = U, \quad v = w = 0, \qquad & \text{on } z = H_1(y), \\ u = v = w = 0, \qquad & \text{on } z = H_2(x). \end{aligned}$$

Finally, we assume that the gas pressure reaches its ambient value P_a at the edges of the slider bearing, i.e.

$$p = P_a \qquad \text{on } x = \pm L \text{ or } y = \pm L \,.$$

In order to derive dimensionless equations, we scale x and y on the slider length L, z on the minimum gap height h_0, streamwise and spanwise components of velocity u and v on U, the normal velocity w on $h_0 U/L$, density ρ on its ambient value $\rho_a = P_a/(RT)$, and write our problem in terms of a dimensionless

gauge pressure $(p - P_a)/(\mu UL/h_0^2)$. With these choices, the dimensionless versions of (1), (2) and (3) can be written in as

$$\begin{aligned}
(\rho u)_x + (\rho v)_y + (\rho w)_z &= 0, \\
\rho \mathrm{Re}^* \left(u u_x + v u_y + w u_z\right) + p_x &= u_{zz} + \delta^2 \left(u_{xx} + u_{yy}\right) + \frac{\delta^2}{3}\left(u_{xx} + v_{yx} + w_{zx}\right), \\
\rho \mathrm{Re}^* \left(u v_x + v v_y + w v_z\right) + p_y &= v_{zz} + \delta^2 \left(v_{xx} + v_{yy}\right) + \frac{\delta^2}{3}\left(u_{xy} + v_{yy} + w_{zy}\right), \\
\rho \mathrm{Re}^* \left(u w_x + v w_y + w w_z\right) + \frac{1}{\delta^2} p_z &= w_{zz} + \delta^2 \left(w_{xx} + w_{yy}\right) + \frac{1}{3}\left(u_{xz} + v_{yz} + w_{zz}\right),
\end{aligned} \tag{4}$$

and

$$\rho = 1 + \left(\frac{\Lambda}{6}\right) p, \tag{5}$$

where $\delta = h_0/L$ is the aspect ratio of the fluid domain, Re^* is the reduced Reynolds number, and Λ is the bearing number (defined earlier). In terms of the dimensionless variables, the boundary conditions become

$$\begin{aligned}
u = 1, \quad v = w = 0, \qquad & \text{on } z = h_1(y), \\
u = v = w = 0, \qquad & \text{on } z = h_2(x).
\end{aligned}$$

where $h_1 = H_1/h_0$ and $h_2 = H_2/h_0$, and

$$p = 0 \qquad \text{on } x = \pm 1 \text{ or } y = \pm 1 .$$

For the analysis below, we consider the Stokes régime where Re^* is small so that the convective terms on the left-hand-side of the momentum equations are dropped, and take $\Lambda = O(1)$. We also consider the case $\delta \ll 1$, and use the fact that the longitudinal roughness of the disk scales on the gap thickness h_0, while the pressure variations due to the slider include a dependence on the scale of the slider L. From this we consider a fast variable in the spanwise direction, $\eta = y/\delta$, and a slow variable, y, and assume that these two variables are independent so that

$$(\cdot)_y \longrightarrow (\cdot)_y + \frac{1}{\delta}(\cdot)_\eta \tag{6}$$

In addition, we will perform a homogenization analysis in which we require that the dependent variables are periodic in fast variable η over some spatial period $\ell = \lambda/h_0$, where λ is the dimensional scale of the longitudinal roughness. With these assumptions, the equations for mass and momentum become

$$\begin{aligned}
(\rho u)_x + (\rho v)_y + \frac{1}{\delta}(\rho v)_\eta + (\rho w)_z &= 0, \\
p_x = u_{zz} + \delta^2 \left(u_{xx} + u_{yy} + \frac{2}{\delta} u_{y\eta} + \frac{1}{\delta^2} u_{\eta\eta}\right) &+ \frac{\delta^2}{3}\left(u_{xx} + v_{yx} + \frac{1}{\delta} v_{\eta x} + w_{zx}\right), \\
p_y + \frac{1}{\delta} p_\eta = v_{zz} + \delta^2 \left(v_{xx} + v_{yy} + \frac{2}{\delta} v_{y\eta} + \frac{1}{\delta^2} v_{\eta\eta}\right) & \\
+ \frac{\delta^2}{3}\left(u_{xy} + \frac{1}{\delta} u_{x\eta} + v_{yy} + \frac{2}{\delta} v_{y\eta} + \frac{1}{\delta^2} v_{\eta\eta} + w_{zy} + \frac{1}{\delta} w_{z\eta}\right), & \\
\frac{1}{\delta^2} p_z = w_{zz} + \delta^2 \left(w_{xx} + w_{yy} + \frac{2}{\delta} w_{y\eta} + \frac{1}{\delta^2} w_{\eta\eta}\right) &+ \frac{1}{3}\left(u_{xz} + v_{yz} + \frac{1}{\delta} v_{\eta z} + w_{zz}\right),
\end{aligned}$$

(It is noted that the leading order terms amongst the convective terms in (4) are of size Re^*/δ in view of (6), but these are still taken to be small and are neglected.)

We now assume that (u, v, w, p) can be expanded in regular perturbation expansions in δ, namely,

$$\begin{aligned} u &= u_0(x, y, \eta, z) + \delta u_1(x, y, \eta, z) + \dots \\ v &= v_0(x, y, \eta, z) + \delta v_1(x, y, \eta, z) + \dots \\ w &= v_0(x, y, \eta, z) + \delta w_1(x, y, \eta, z) + \dots \\ p &= p_0(x, y, \eta, z) + \delta p_1(x, y, \eta, z) + \dots \end{aligned}$$

and then substitute these into the governing equations and equate terms in powers of δ. (No expansion is needed for the ρ as the equation of state in (5) is used to eliminate the density in favor of the pressure p.) The leading-order set of equations are

$$\left(\left(1 + \frac{\Lambda}{6} p_0\right) v_0\right)_\eta = 0, \tag{7}$$

$$p_{0,x} = u_{0,\eta\eta} + u_{0,zz}, \tag{8}$$

$$p_{0,\eta} = 0, \tag{9}$$

$$p_{0,z} = 0 \tag{10}$$

Equations (9) and (10) imply that $p_0 = p_0(x, y)$ so that (7) reduces to $v_{0,\eta} = 0$ which implies $v_0 = v_0(x, y, z)$. The problem for u_0 is a Poisson equation with boundary conditions

$$u_0 = 1 \text{ on } z = h_1(\eta), \qquad u_0 = 0 \text{ on } z = h_2(x), \qquad \text{and } u_0 \text{ is } \ell\text{-periodic in } \eta.$$

At next order the equations are

$$\frac{\Lambda}{6} v_0 p_{1,\eta} + \left(1 + \frac{\Lambda}{6} p_0\right) v_{1,\eta} = -\left(\left(1 + \frac{\Lambda}{6} p_0\right) u_0\right)_x - \left(\left(1 + \frac{\Lambda}{6} p_0\right) v_0\right)_y - \left(1 + \frac{\Lambda}{6} p_0\right) w_{0,z}, \tag{11}$$

$$p_{1,x} - u_{1,\eta\eta} - u_{1,zz} = 2u_{0,y\eta}, \tag{12}$$

$$p_{1,\eta} = -p_{0,y} + v_{0,zz}, \tag{13}$$

$$p_{1,z} = 0 \tag{14}$$

From (14) we have that $p_1 = p_1(x, y, \eta)$, and from (13) we may integrate once to give

$$p_1 = (-p_{0,y} + v_{0,zz})\,\eta + P_1(x, y).$$

Since p_1 is assumed to be ℓ-periodic in η, we have

$$v_{0,zz} = p_{0,y}.$$

We may integrate this equation twice in z and use the boundary conditions $v_0 = 0$ on $z = h_1$ and $z = h_2$ to give

$$v_0 = \frac{1}{2} p_{0,y}\,(z - h_1)\,(z - h_2).$$

Recall that h_1 depends on η whereas it was found above that v_0 is independent of η. Assuming that h_1 is nonzero, we conclude that $p_{0,y} = 0$ so that v_0 remains independent of η. This implies that $p_0 = p_0(x)$ and that v_0 is identically zero, and thus p_1 is a function of x and y (at most). With these simplifications in hand, (11) reduces to

$$\left(1 + \frac{\Lambda}{6} p_0\right) v_{1,\eta} = -\left(\left(1 + \frac{\Lambda}{6} p_0\right) u_0\right)_x - \left(1 + \frac{\Lambda}{6} p_0\right) w_{0,z}. \tag{15}$$

We now consider the integral of (15) over the domain $-\ell/2 < \eta < \ell/2$ and $h_1(\eta) < z < h_2(x)$ to get

$$\begin{aligned} \left(1 + \frac{\Lambda}{6} p_0\right) \int_{-\ell/2}^{\ell/2} \int_{h_1(\eta)}^{h_2(x)} v_{1,\eta}\, dz d\eta = &-\int_{-\ell/2}^{\ell/2} \int_{h_1(\eta)}^{h_2(x)} \left(\left(1 + \frac{\Lambda}{6} p_0\right) u_0\right)_x dz d\eta \\ &- \left(1 + \frac{\Lambda}{6} p_0\right) \int_{-\ell/2}^{\ell/2} \int_{h_1(\eta)}^{h_2(x)} w_{0,z}\, dz d\eta. \end{aligned} \tag{16}$$

Since $w_0 = 0$ at both $z = h_1$ and h_2, it is clear that the second integral on the right-hand-side of (16) is zero. The integral on the left-hand-side of (16) also vanises by the following argument. We assume here that $h_1(\eta)$ is even about $\eta = 0$ and that $z = h_1(\eta)$, restricted to the half interval $0 < \eta < \ell/2$, has an inverse function defined by $\eta = g_1(z)$, say. Let us switch the order of integration in this integral to get

$$\int_{-\ell/2}^{\ell/2}\int_{h_1(\eta)}^{h_2(x)} v_{1,\eta}\,dzd\eta = \int_{h_1(-\ell/2)}^{h_1(0)}\int_{-\ell/2}^{-g_1(z)} v_{1,\eta}\,d\eta dz + \int_{h_1(\ell/2)}^{h_1(0)}\int_{g_1(z)}^{\ell/2} v_{1,\eta}\,d\eta dz + \int_{h_1(0)}^{h_2(x)}\int_{-\ell/2}^{\ell/2} v_{1,\eta}\,d\eta dz. \quad (17)$$

Based on symmetry of $h_1(\eta)$ on $-\ell/2 < \eta < \ell/2$ and with periodicity of v_1 in η, the first two integrals on the right-hand-side of (17) add to zero identically, while the third integral is itself zero by periodicity.

Hence, the leading order effective Reynolds equation to solve involves a Poisson problem for $u_0(x,\eta,z)$ given by

$$u_{0,\eta\eta} + u_{0,zz} = p_{0,x}, \qquad -\ell/2 < \eta < \ell/2, \quad h_1(\eta) < z < h_2(x),$$

with boundary conditions

$$u_0 = 1 \text{ on } z = h_1(\eta), \quad u_0 = 0 \text{ on } z = h_2(x), \quad \text{and } u_0 \text{ is } \ell\text{-periodic in } \eta$$

for $0 < x < 1$, coupled to a problem for $p_0(x)$ given by

$$\int_{-\ell/2}^{\ell/2}\int_{h_1(\eta)}^{h_2(x)} \left(\left(1 + \frac{\Lambda}{6}p_0\right)u_0\right)_x dzd\eta = 0, \qquad p_0(0) = p_0(1) = 0. \quad (18)$$

This coupled problem may be broken down into two stages. For the first stage, let $\phi(x,\eta,z)$ and $\psi(x,\eta,z)$ solve

$$\phi_{\eta\eta} + \phi_{zz} = 1, \qquad -\ell/2 < \eta < \ell/2, \quad h_1(\eta) < z < h_2(x),$$

with boundary conditions

$$\phi = 0 \text{ on } z = h_1(\eta), \quad \phi = 0 \text{ on } z = h_2(x), \quad \text{and } \phi \text{ is } \ell\text{-periodic in } \eta$$

and

$$\psi_{\eta\eta} + \psi_{zz} = 0, \qquad -\ell/2 < \eta < \ell/2, \quad h_1(\eta) < z < h_2(x),$$

with boundary conditions

$$\psi = 1 \text{ on } z = h_1(\eta), \quad \psi = 0 \text{ on } z = h_2(x), \quad \text{and } \psi \text{ is } \ell\text{-periodic in } \eta$$

so that the solution of the Poisson problem for u_0 is given by

$$u_0(x,\eta,z) = p_{0,x}(x)\phi(x,\eta,z) + \psi(x,\eta,z). \quad (19)$$

The problems for ϕ and ψ may be solved independently of the pressure p_0. Once these are found, then we may use (19) in (18) to obtain a two-point boundary-value problem to solve for p_0, namely,

$$K_1\left[\left(1 + \frac{\Lambda}{6}p_0\right)p_{0,x}\right]_x + D_1\left[\left(1 + \frac{\Lambda}{6}p_0\right)p_{0,x}\right] + K_2\frac{\Lambda}{6}p_{0,x} + D_2\left(1 + \frac{\Lambda}{6}p_0\right) = 0, \qquad 0 < x < 1, \quad (20)$$

with $p_0(0) = p_0(1) = 0$. The coefficient functions of the ODE are defined by

$$\begin{aligned} K_1(x) &= \int_{-\ell/2}^{\ell/2}\int_{h_1(\eta)}^{h_2(x)} \phi\,dzd\eta, \qquad D_1(x) = \int_{-\ell/2}^{\ell/2}\int_{h_1(\eta)}^{h_2(x)} \phi_x\,dzd\eta, \\ K_2(x) &= \int_{-\ell/2}^{\ell/2}\int_{h_1(\eta)}^{h_2(x)} \psi\,dzd\eta, \qquad D_2(x) = \int_{-\ell/2}^{\ell/2}\int_{h_1(\eta)}^{h_2(x)} \psi_x\,dzd\eta. \end{aligned} \quad (21)$$

The second stage involves solving the problem for p_0.

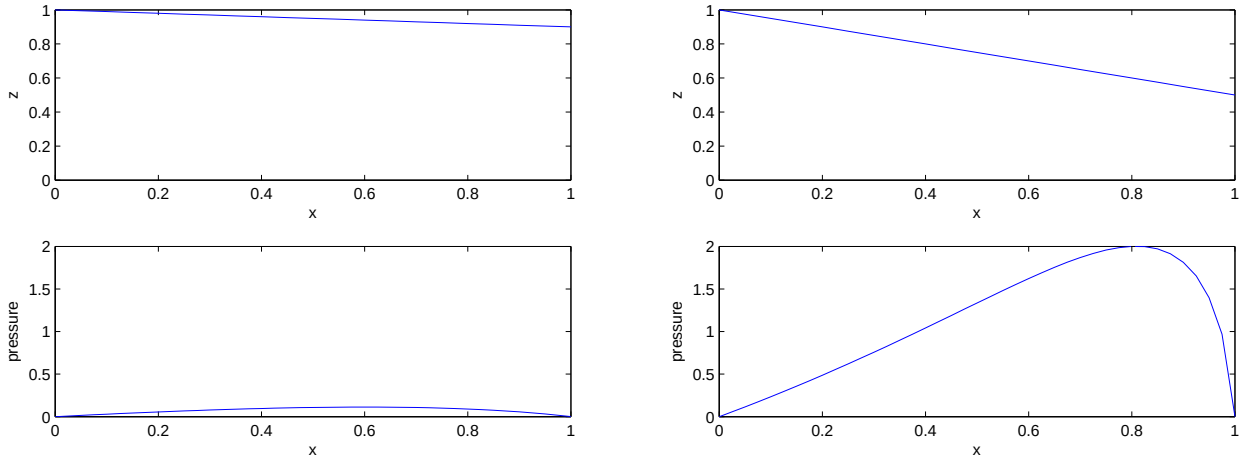

Figure 3: Numerical solutions for the pressure in the gap for $\Lambda = 10$. Slider function $h_2(x) = 1 - \alpha x$ (top) and the corresponding gap pressure $p_0(x)$ (bottom) for the case $\alpha = 0.1$ (left) and $\alpha = 0.5$ (right).

2.2 Sample calculations

In this section, we discuss some sample calculations for the leading-order pressure p_0 in the gap. For these calculations, we choose

$$h_1(\eta) = 0.2\cos(2\pi\eta) \quad \text{for} \quad -1/2 \le \eta \le 1/2\,,$$

and take

$$h_2(x) = 1 - \alpha x\,, \text{ where } \alpha \text{ is the slope of the slider.}$$

The numerical calculations follow the two-stage procedure discussed above. In the first stage, the problems for ϕ and ψ are solved numerically at 21 uniformly spaced grid points in the x-direction. At each x position, the elliptic problems are solved by first mapping the domain $-1/2 \le \eta \le 1/2\,,\ h_1(\eta) \le z \le h_2(x)$ to the computational domain $-1/2 \le \bar{\eta} \le 1/2\,,\ 0 \le \bar{z} \le 1$ using

$$\bar{\eta} = \eta, \qquad \bar{z} = \frac{z - h_1(\eta)}{h_2(x) - h_1(\eta)}.$$

The mapped equations are solved for ϕ and ψ using a uniform grid in $(\bar{\eta}, \bar{z})$ with 50 grid cells in both directions. Once ϕ and ψ are known on the grid, the coefficient functions K_1, K_2, D_1 and D_2 given by the integrals in (21) are computed using trapezoidal-rule approximations. The second stage of the calculation is now performed by solving the two-point boundary-value problem for p_0 in (20) with $\Lambda = 10$ using a standard second-order finite-difference approximation of the equations on the uniform grid in x. (A smaller value for the bearing number is used to avoid the sharp boundary layer at $x = 1$.)

Figure 3 shows two calculations, one for the slope $\alpha = 0.1$ of the slider function $h_2(x)$ and the other for $\alpha = 0.5$. As expected, the gap pressure increases from zero at the inlet ($x = 0$) and achieves a maximum near the outlet of the slider before decreasing back to zero at $x = 1$. Also, we observe that the maximum value for the pressure increases with increasing α as expected. The behavior of the pressure is qualitatively similar to that given by the solution of the Reynolds equation along the centerline $y = 0$ of an inclined slider.

As a final calculation for this problem, we show in Figure 4 the results for the case

$$h_2(x) = 1 - \alpha x - \beta\sin(2\pi x)\,, \text{ where } \alpha = 0.5 \text{ and } \beta = 0.2\,.$$

For this choice, the local increase in $h_2(x)$ in the middle of the interval between 0 and 1 creates a broader region of near-maximum pressure in the gap. This would lead to a larger lift on the slider for this case.

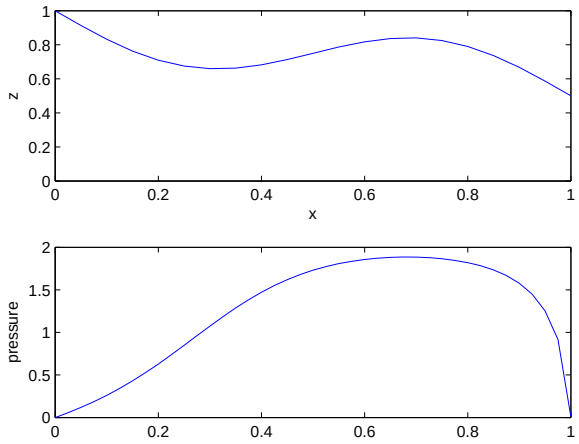

Figure 4: Numerical solutions for the pressure in the gap for $\Lambda = 10$. Slider function $h_2(x) = 1 - \alpha x - \beta \sin(2\pi x)$ (top) and the corresponding gap pressure $p_0(x)$ (bottom) for the case $\alpha = 0.5$ and $\beta = 0.2$.

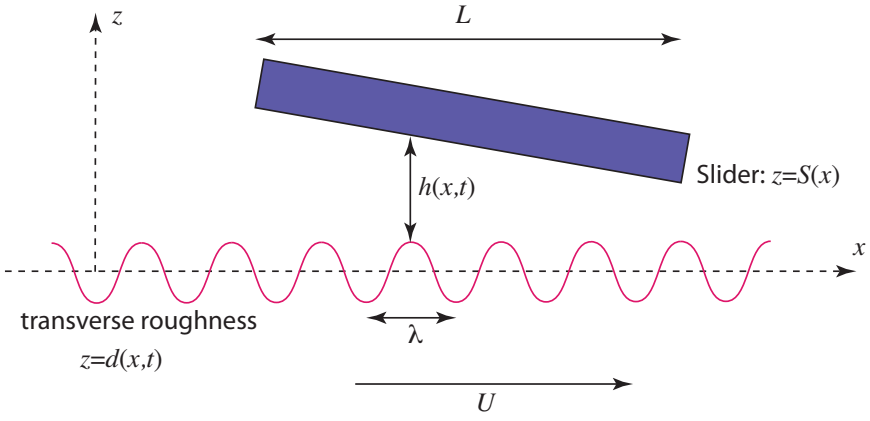

Figure 5: Flow geometry for the slider problem with transverse roughness. The slider has length given by L and moves with speed U. The gap height is $h(x,t)$ and the period of the transverse roughness is λ.

3 Transverse Roughness

The flow geometry for the problem of a slider traveling over a disk with transverse roughness, the so-called speed-bump problem, is shown in Figure 5. The length of the slider is L and its shape is given by $z = S(x)$. The slider travels along the disk at a speed U. The roughness of the disk is given by $z = d(x,t)$ and it is assumed that the length scale of the roughness is λ. The gap height is taken to be

$$h(x,t) = s(t) + S(x) - d(x,t),$$

where $s(t)$ is the vertical displacement of the slider from $z = S(0)$, and whose time-dependent behavior may be considered to balance an applied vertical load on the slider. It is assumed that the pressure $p(x,t)$ in the gap satisfies the compressible Reynolds equation

$$(ph)_t + \frac{1}{2}(ph)_x = \frac{1}{2\Lambda}(ph^3 p_x)_x, \qquad 0 < x < 1, \qquad p(0,t) = p(1,t) = 1. \tag{22}$$

where Λ is the bearing number. Here, the (scaled) pressure p is chosen to be an *absolute* pressure in contrast to the *gauge* pressure used in the previous analysis of longitudinal roughness. Thus, p is equal to 1 on the boundary (and not zero as before). In dimensionless units the disk moves with speed equal to 1, and it is assumed that the roughness has the form of a traveling wave (also with speed equal to 1) and is given by

$$d(x,t) = D\left(\frac{x-t}{\epsilon}\right).$$

where $\epsilon = \lambda/L$.

This problem was studied in two ways. Firstly the behavior of the flow in the limit of large Λ was sought, and then the behavior of the flow was considered for the case of a very rough surface, i.e. $\epsilon \ll 1$, but with order one Λ.

3.1 Large bearing number analysis

In the limit $\Lambda \gg 1$, the leading-order, outer solution of (22) has the form

$$ph = f\left(x - \frac{t}{2}\right), \tag{23}$$

where f is determined by the conditions at the inlet, $x = 0$, for $t \geq 2$. At the outlet, $x = 1$, there is a boundary layer of thickness $1/\Lambda$ needed for p to satisfy the boundary condition $p(1,t) = 1$, but we will not consider this solution in the subsequent analysis because it has a small effect on the force generated on the slider. Applying the conditions at the inlet to (23) gives

$$f(\bar{t}) = S(0) + s(-2\bar{t}) - D\left(2\bar{t}/\epsilon\right),$$

for some dummy variable $\bar{t}$, so that the outer solution is

$$p(x,t) = \frac{S(0) + s(t-2x) - D\left((2x-t)/\epsilon\right)}{S(x) + s(t) - D\left((x-t)/\epsilon\right)} \tag{24}$$

to leading order. A simple model for the behavior of $s(t)$ for the slider assumes that difference between the force generated by the gap pressure and the applied load on the slider drives a dynamical system consisting of a spring with constant k and a viscous damper with constant γ. The ODE for this system is

$$M\frac{d^2 s}{dt^2} + \gamma\frac{ds}{dt} + k(s - s_0) = \int_0^1 (p-1)\,dx - F, \tag{25}$$

where M is the mass of the slider, s_0 is an equilibrium height, F is the applied downward load, and p is given by (24).

ϵ	$I(\epsilon)$	$I_\infty(\epsilon)$	Error
0.04	0.4043	0.4048	$1.2\text{e}-3$
0.01	0.4155	0.4156	$6.1\text{e}-5$
0.0025	0.4221	0.4254	$7.7\text{e}-3$

Table 2: Values of the integral of $(p-1)$ from $x=0$ to $x=1$ at $t=2$.

The leading order solution in (23) is a valid approximation of the solution of the Reynolds equations provided the diffusive term on the right-hand-side of (22) is small. This is true for large values of Λ provided $(ph^3p_x)_x$ is $O(1)$. The approximation breaks down, as mentioned previously, near the boundary layer at $x=1$, but would also be invalid for the case of very rapid surface roughness when ϵ is very small, i.e. when $1/\Lambda \sim \epsilon$. To give an illustration of the behavior of $p(x,t)$ as ϵ becomes small, we consider the case

$$s(t)=0, \qquad S(x)=2-x, \qquad D\left(\frac{x-t}{\epsilon}\right)=\frac{3}{10}\sin\left(\frac{x-t}{\epsilon}\right),$$

and compare numerical solutions of the full equations in (22) with the approximate solution in (23). Figure 6 shows this comparison at $t=2$ for $\Lambda=10^5$ and for $\epsilon=1/25$, $1/100$ and $1/400$. We note that as ϵ decreases the number of wiggles in the pressure increases. For $\epsilon=0.04$ there is very good agreement between the approximate solution (red curve) and the solution of the full equation (blue curve); the diffusive term is small for this relatively large value of ϵ except near the boundary at $x=1$. (The boundary layer at $x=1$ is so narrow that it is not visible on the scale of the plots.) For $\epsilon=0.01$ and $\epsilon=0.0025$ the agreement is not as good, especially near local minima and maxima where the curvature is large and the diffusive term in (22) becomes significant. The effect of this term is to smooth out the extrema as is seen clearly in the enlarged view of the behavior near $x=0$ for $\epsilon=0.0025$. For even smaller values of ϵ, equal to 5×10^{-5} say, according to the values listed in Table 1, we would expect a large difference between the approximate solution and the solution of the full equations since $1/\Lambda=10^{-5}\approx\epsilon$.

Despite the difference in the solutions for pressure for small values of ϵ, the integral in (25) may still be obtained with reasonable accuracy since it appears that the contributions of this difference to the integral may cancel. In Table 2, we list the computed values of the integral of $(p-1)$ from $x=0$ and $x=1$ at $t=2$ for each value of ϵ. The value of the integral obtained from solution of the full equations with $\Lambda=10^5$ is denoted by $I(\epsilon)$ whereas the value obtained from the approximate solution in (23) is denoted by $I_\infty(\epsilon)$. For all three values of ϵ considered, the relative error between these two values is small.

No further analysis of the speed-bump problem in the limit of large bearing number is considered here, but there are further relevant details in [3].

3.2 Homogenized Reynolds Equation

The next problem considered is how to incorporate into the model the very rapidly varying surface roughness. The starting point for the analysis is the unsteady compressible Reynolds equation in (22), but now with height given by

$$h(x,t)=S(x)-D\left(\frac{x-t}{\epsilon}\right). \tag{26}$$

Here, $s(t)$ is set to zero and we assume that D is a periodic function of its argument (with period equal to 1) and that $\epsilon \ll 1$. (We note that while $s=0$ here for simplicity, a nonzero function could be readily incorporated in the following analysis.) We will consider fast and slow scales in space given by $\xi=x/\epsilon$ and x, respectively, and a fast time scale given by $\tau=t/\epsilon$. In the usual multiple-scale analysis, we consider ξ and x to be independent, so that

$$(\cdot)_x \longrightarrow (\cdot)_x+\frac{1}{\epsilon}(\cdot)_\xi\ ,$$

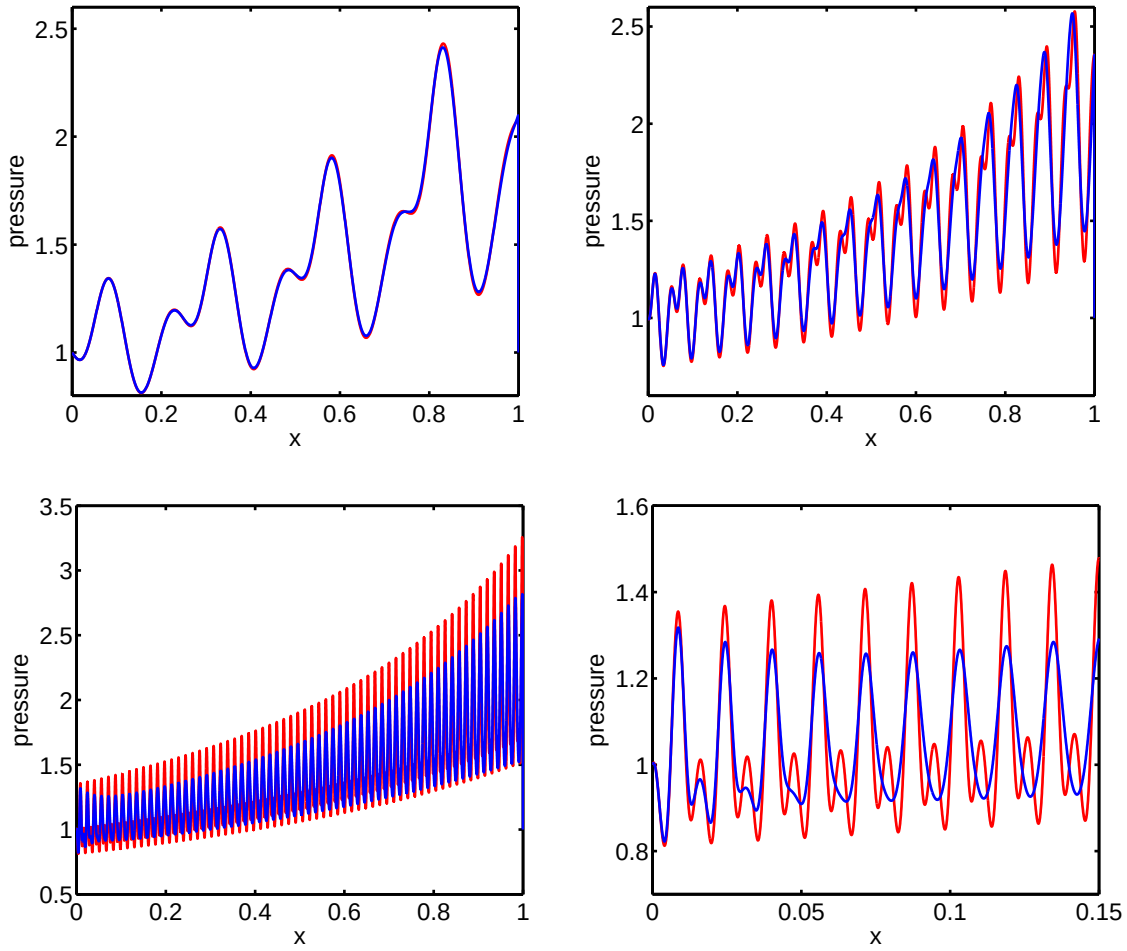

Figure 6: Comparison of the pressure in the gap given by the approximate solution in (23) (red curves) and solution of the full equations in (22) with $\Lambda = 10^5$ (blue curves) at $t = 2$. The top left plot is $\epsilon = 0.04$, the top right plot is $\epsilon = 0.01$ and the bottom plots are both $\epsilon = 0.0025$. The bottom right plot is an enlarged view of the $\epsilon = 0.0025$ solution.

similar to the approach used in the previous section. For the present analysis, the Reynolds equation then becomes

$$\frac{1}{\epsilon}(ph)_\tau + \frac{1}{2}(ph)_x + \frac{1}{2\epsilon}(ph)_\xi = \frac{1}{2\Lambda}(php_x)_x + \frac{1}{2\epsilon\Lambda}(php_\xi)_x + \frac{1}{2\epsilon\Lambda}(php_x)_\xi + \frac{1}{2\epsilon^2\Lambda}(php_\xi)_\xi, \tag{27}$$

with

$$h(x,\xi,\tau) = S(x) - D(\xi - \tau)\,. \tag{28}$$

We now consider the asymptotic expansion

$$p(x,\xi,\tau) = p_0 + \epsilon p_1 + \epsilon^2 p_2 + \ldots$$

in (27) and then collect terms in the same power of ϵ.

Terms at $O(\epsilon^{-2})$:

The equation at this order is

$$\frac{1}{2\Lambda}\left(p_0 h^3 p_{0,\xi}\right)_\xi = 0\,.$$

Integrating this once in ξ gives

$$p_0 h^3 p_{0,\xi} = f(x,\tau),$$

for some function $f(x,\tau)$. We note that $p_0 p_{0,\xi} = (p_0^2)_\xi/2$ so that we may integrate again to give

$$p_0^2 = 2f(x,\tau)\int_0^\xi \frac{1}{h^3}\,d\xi + \left[g(x,\tau)\right]^2,$$

for some function $g(x,\tau)$. The method of multiple scales now requires that the solution remain bounded as $\xi \to \pm\infty$. This can be done directly or, as is often assumed and is equivalent in this case, the solution can be made to be periodic in ξ. Following the latter approach (see [1]), we conclude that $f = 0$ so that p_0 is independent of ξ, namely,

$$p_0 = g(x,\tau).$$

Terms at $O(\epsilon^{-1})$:

The equation at this order is

$$(p_0 h)_\tau + \frac{1}{2}\left(p_0 h\right)_\xi = \frac{1}{2\Lambda}\left(p_0 h^3 p_{0,\xi}\right)_x + \frac{1}{2\Lambda}\left(p_0 h^3 p_{0,x}\right)_\xi + \frac{1}{2\Lambda}\left(p_1 h^3 p_{0,\xi}\right)_\xi + \frac{1}{2\Lambda}\left(p_0 h^3 p_{1,\xi}\right)_\xi\,.$$

We exploit the fact that p_0 is independent of ξ to re-write this as

$$\frac{1}{2\Lambda}\left(p_0 h^3 p_{1,\xi}\right)_\xi = (p_0 h)_\tau + \frac{1}{2}\left(p_0 h\right)_\xi - \frac{1}{2\Lambda}\left(p_0 h^3 p_{0,x}\right)_\xi,$$

and then note that the form of h ensures that $h_\tau = -h_\xi$ so that

$$\frac{1}{2\Lambda}p_0\left(h^3 p_{1,\xi}\right)_\xi = h p_{0,\tau} - \frac{1}{2}p_0 h_\xi - \frac{1}{2\Lambda}p_0 p_{0,x}\left(h^3\right)_\xi\,. \tag{29}$$

As before, we can integrate this equation and require that p_1 remains bounded as $\xi \to \pm\infty$. Again this is equivalent to ensuring p_1 is periodic. To make $p_{1,\xi}$ periodic we require that all terms on the right hand side of (29) are periodic in ξ with zero mean. Because h is periodic but does not have zero mean and p_0 depends only on x and τ (at most), all but the first term on the right hand side satisfies the requirement. Therefore we need to impose the condition that

$$h p_{0,\tau} = 0,$$

and so p_0 only depends on x, e.g.

$$p_0 = G(x).$$

The remaining terms in (29) may then be integrated to give

$$\frac{1}{2\Lambda}p_0h^3p_{1,\xi} = \frac{1}{2\Lambda}p_0K(x,\tau) - \frac{1}{2}p_0h - \frac{1}{2\Lambda}p_0p_{0,x}h^3,$$

where $K(x,\tau)$ is some function. Since $p_{1,\xi}$ must be periodic and have zero mean so that p_1 is periodic, we choose K such that

$$K(x,\tau)\int_0^1 \frac{1}{h^3}\,d\xi - \Lambda\int_0^1 \frac{1}{h^2}\,d\xi - p_{0,x} = 0,$$

which implies

$$K(x,\tau) = \frac{\Lambda\int_0^1 h^{-2}\,d\xi + p_{0,x}}{\int_0^1 h^{-3}\,d\xi}.$$

Using K in the expression for $p_{1,\xi}$ we can integrate once again to find

$$p_1 = \frac{\Lambda\int_0^1 h^{-2}\,d\xi\int_0^\xi h^{-3}\,d\xi}{\int_0^1 h^{-3}\,d\xi} - \Lambda\int_0^\xi h^{-2}\,d\xi + p_{0,x}\left(-\xi + \frac{\int_0^\xi h^{-3}\,d\xi}{\int_0^1 h^{-3}\,d\xi}\right) + J(x,\tau), \tag{30}$$

where $J(x,\tau)$ is some function. For the purposes of making the subsequent algebra tolerable we shall introduce some additional notation and write (30) in the form

$$p_1 = B(x,\tau,\xi) + C(x,\tau,\xi)p_{0,x} + J(x,\tau), \tag{31}$$

where

$$B = \Lambda\left(\frac{\int_0^1 h^{-2}\,d\xi\int_0^\xi h^{-3}\,d\xi}{\int_0^1 h^{-3}\,d\xi} - \int_0^\xi h^{-2}\,d\xi\right), \qquad C = -\xi + \frac{\int_0^\xi h^{-3}\,d\xi}{\int_0^1 h^{-3}\,d\xi},$$

and we note that $B(\xi)$ and $C(\xi)$ are periodic in ξ.

Terms at $O(1)$:

The equation at this order is

$$(p_1h)_\tau + \frac{1}{2}(p_0h)_x + \frac{1}{2}(p_1h)_\xi = \frac{1}{2\Lambda}(p_0h^3p_{0,x})_x + \frac{1}{2\Lambda}(p_0h^3p_{1,\xi})_x + \frac{1}{2\Lambda}(p_0h^3p_{1,x})_\xi + \frac{1}{2\Lambda}(p_1h^3p_{0,x})_\xi + \frac{1}{2\Lambda}(p_0h^3p_{2,\xi})_\xi + \frac{1}{2\Lambda}(p_1h^3p_{1,\xi})_\xi.$$

Once again we impose the condition that $p_{2,\xi}$ be periodic with zero mean so that p_2 can be periodic. All of the terms that are derivatives of ξ already satisfy this property. We impose that the mean of the remaining terms is zero by requiring that the integral in ξ over a period for all of the remaining terms, not containing p_2, be zero. This condition gives us

$$\int_0^1\left[(p_1h)_\tau + \frac{1}{2}(p_0h)_x - \frac{1}{2\Lambda}(p_0h^3p_{0,x})_x - \frac{1}{2\Lambda}(p_oh^3p_{1,\xi})_x\right]d\xi = 0. \tag{32}$$

We can now substitute the expression in (31) into this equation. Because we have previously found that p_0 is independent of τ this imposes a condition on p_1 (thereby restricting $J(x,\tau)$ although we shall not actually need to find this restriction explicitly) in order that a solution exists to the problem. This condition is most easily determined by noting that we require p_1 to be periodic in τ (as well as in ξ) and this can only occur if the integral of the equation in (32) is zero over one time period. The problem is therefore

$$\int_0^1\int_0^1\left[\frac{1}{2}(p_0h)_x - \frac{1}{2\Lambda}(p_0h^3p_{0,x})_x - \frac{1}{2\Lambda}\left(p_0h^3\left(B_\xi + C_\xi\,p_{0,\xi}\right)\right)_\xi\right]d\xi d\tau = 0. \tag{33}$$

We may now use the definitions of $B(x,\tau,\xi)$ and $C(x,\tau,\xi)$ in (33) to derive a homogenized equation for $p_0(x)$ that involves various averages of $h(x,\tau,\xi)$ over the fast variables ξ and τ. The equation (with boundary conditions) is

$$\frac{1}{2}(p_0\bar{h})_x = \frac{1}{2\Lambda}(p_0\hat{h}^3p_{0,x})_x, \qquad 0<x<1, \qquad p_0(0,t) = p_0(1,t) = 1, \tag{34}$$

where

$$\bar{h} = \int_0^1 \left\{ 2\int_0^1 h\, d\xi - \frac{\int_0^1 h^{-2}\, d\xi}{\int_0^1 h^{-3}\, d\xi} \right\} d\tau, \qquad \hat{h}^3 = \int_0^1 \left\{ \frac{1}{\int_0^1 h^{-3}\, d\xi} \right\} d\tau. \tag{35}$$

We see that the steady problem for $p_0(x)$ retains the same form as the steady Reynolds equation, but with new coefficients involving certain averages of the gap height.

Lastly, we note that the homogenized coefficients $\bar{h}$ and $\hat{h}$ given in (35) involve integrals of h of the form

$$I_m = \int_0^1 h^m\, d\xi, \qquad \text{for } m = 1\,,\ -2 \text{ and } -3\,.$$

For the simple case with $m = 1$ and h given in (28), we have

$$I_1 = \int_0^1 \big(S(x) - D(\xi - \tau)\big)\, d\xi = S(x) - \int_0^1 D(\xi - \tau)\, d\xi = S(x),$$

assuming that D is 1-periodic with zero mean. For the case with $m = -2$, we use

$$\frac{1}{h^2} = \frac{1}{(S-D)^2} = \frac{1}{S^2}\left(\frac{1}{1 - D/S}\right)^2 = \frac{1}{S^2}\sum_{k=0}^{\infty}(k+1)\left(\frac{D}{S}\right)^k,$$

to find

$$I_{-2} = \frac{1}{S(x)^2}\sum_{k=0}^{\infty}\frac{(k+1)}{S(x)^k}\int_0^1 \big(D(\xi-\tau)\big)^k\, d\xi = \frac{1}{S(x)^2}\left(1 + O(\Delta^2)\right), \tag{36}$$

where $\Delta = \max|D/S| < 1$ gives the relative size of the roughness. Similarly, for $m = -3$ we find

$$I_{-3} = \frac{1}{S(x)^3}\sum_{k=0}^{\infty}\frac{(k+1)(k+2)}{2S(x)^k}\int_0^1 \big(D(\xi-\tau)\big)^k\, d\xi = \frac{1}{S(x)^3}\left(1 + O(\Delta^2)\right). \tag{37}$$

The implication of these results is two fold. First, we see that $\bar{h}$ and $\hat{h}$ both have the form $S(x)(1+O(\Delta^2))$ so that the corrections in (34) due to the homogenization are second order in Δ. Second, we note that the summation formulas in (36) and (37) provide a means to compute $\bar{h}$ and $\hat{h}$ analytically for some choices of the roughness function D (if D is trigonometric for example).

3.3 A sample calculation

We now consider the long-time solution of the original time-dependent problem in (22) with a choice for the gap height $h(x,t)$ in (26), and compare it with the steady solution of the homogenized problem in (34). For this exercise, we pick

$$h(x,t) = S(x) - D\left(\frac{x-t}{\epsilon}\right) = 2 - x - \frac{3}{10}\sin\left(\frac{x-t}{\epsilon}\right), \qquad \epsilon = 0.01, \qquad \Lambda = 10.$$

The initial condition is taken to be $p(x,0) = 1$, and the equations are solved numerically using 2000 uniformly spaced grid cells on the interval $0 \le x \le 1$ for time t between 0 and t_{final}. The value for t_{final} is chosen to be large enough (equal to 10 in our calculation) so that the solution has reached a quasi-steady state in which the pressure shows small traveling oscillations about a steady solution. The red curves in the two plots in Figure 7 are solutions at $t = 9.9$ and $t = 10$. The blue curve in the plot on the left in the figure is the corresponding numerical solution of the steady homogenized equations (34) using a uniform mesh in x with 200 grid cells. Here, we observe excellent agreement between the average solution of the original time-dependent problem and the steady solution of the homogenized problem. In the right plot of Figure 7, we compare the solution of the original time-dependent problem with that given by (34) but with simpler averages given by

$$\bar{h} = \hat{h} = \int_0^1\int_0^1 h(x,\xi,\tau)\, d\xi d\tau. \tag{38}$$

We note that this choice, which does not make use of the averages given by the homogenization analysis, results in a much poorer agreement with the time-dependent solution.

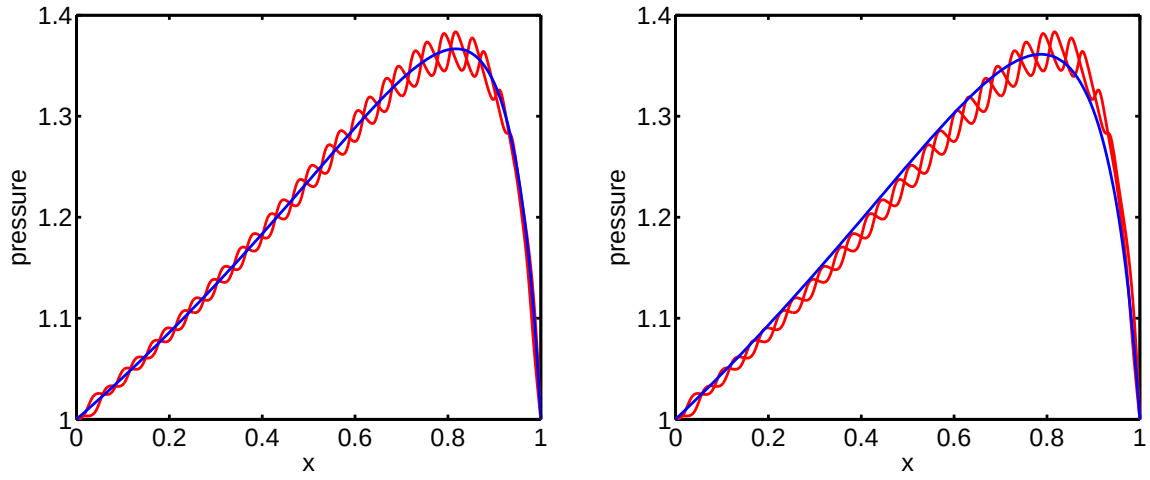

Figure 7: Comparison of the pressure in the gap given by the time-dependent Reynolds equations (red curves) and the pressure given by the steady homogenized equations (blue curves) using $\bar{h}$ and $\hat{h}$ given by (35) (left plot) and by (38) (right plot).

4 Conclusions

We have analyzed the behavior of the flow between a slider bearing and a hard-drive magnetic disk under two types of surface roughness. For both cases the length scale of the roughness along the surface is small as compared to the scale of the slider, so that a homogenization of the governing equations was performed. For the case of longitudinal roughness, we derived a one-dimensional lubrication-type equation for the leading behavior of the pressure in the direction parallel to the velocity of the disk. The coefficients of the equation are determined by solving linear elliptic equations on a domain bounded by the gap height in the vertical direction and the period of the roughness in the span-wise direction. For the case of transverse roughness the unsteady lubrication equations were reduced, following a multiple scale homogenization analysis, to a steady equation for the leading behavior of the pressure in the gap. The reduced equation involves certain averages of the gap height, but retains the same form of the usual steady, compressible lubrication equations. Numerical calculations were performed for both cases, and the solution for the case of transverse roughness was shown be in excellent agreement with a corresponding numerical calculation of the original unsteady equations.

References

[1] E. J. Hinch, Perturbation Methods, Cambridge University Press, Cambridge, 1991.

[2] M. Holmes, Introduction to Perturbation Methods, Springer-Verlag, New York, 1995.

[3] T. P. Witelski, Dynamics of air bearing sliders, Physics of Fluids 10 (1998) 698–708.

[4] M. Jai, B. Bou-Saïd, A comparison of homogenization and averaging techniques for the treatment of roughness in slip-flow-modified Reynolds equation, Journal of Tribology 124 (2002) 327–335.

[5] T. Hayashi, H. Yoshida, Y. Mitsuya, A numerical simulation method to evaluate the static and dynamic characteristics of flying head sliders on patterned disk surfaces, Journal of Tribology 131 (2009) 1–5.